

1 **Robust Genome-Wide Ancestry Inference for Heterogeneous Datasets and**
2 **Ancestry Facial Imaging based on the 1000 Genomes Project**

3
4 Jairui Li^{1,2,*}, Tomas Gonzalez³, Julie D. White³, Karlijne Indencleef^{1,4}, Hanne Hoskens^{1,5}, Alejandra
5 Ortega Castrillon^{1,2}, Nele Nauwelaers^{1,2}, Arslan Zaidi³, Ryan J. Eller⁶, Torsten Günther⁷, Emma M.
6 Svensson⁷, Mattias Jakobsson⁷, Susan Walsh⁶, Kristel Van Steen^{5,8,9}, Mark D. Shriver³, Peter
7 Claes^{1,2,5,10,11*}

8 ¹Medical Imaging Research Center, MIRC, University Hospitals Leuven, Leuven, Belgium

9 ²Department of Electrical Engineering, ESAT/PSI, KU Leuven, Leuven, Belgium

10 ³Department of Anthropology, The Pennsylvania State University, University Park, Pennsylvania, US

11 ⁴Department of Neurosciences, Experimental Otorhinolaryngology, KU Leuven, Leuven, Belgium

12 ⁵Department of Human Genetics, KU Leuven, Leuven, Belgium

13 ⁶Department of Biology, Indiana University-Purdue University Indianapolis, Indianapolis, US

14 ⁷Department of Organismal Biology, Uppsala University, Norbyvägen 18C, 75236, Uppsala, Sweden

15 ⁸Medical Genomics Research Unit, GIGA-R, University of Liège, Belgium

16 ⁹Walloon Excellence in Life sciences and Biotechnology (WELBIO), Belgium;

17 ¹⁰Murdoch Childrens Research Institute, Melbourne, Victoria, Australia

18 ¹¹Department of Biomedical Engineering, University of Oxford, United Kingdom

19 * corresponding authors: Jiarui.li@kuleuven.be, peter.claes@kuleuven.be

20 Medical Imaging Research Center, University Hospitals Leuven, Herestraat 49 – box, 7003, 3000
21 Leuven, Belgium. Phone: +32 16 34 90 24,

22 **Short Title:** Robust Genome-Wide Ancestry Inference for Heterogeneous Datasets

23 **Abstract**

24 Accurate inference of genomic ancestry is critically important in human genetics, epidemiology, and
25 related fields. Geneticists today have access to multiple heterogeneous population-based datasets
26 from studies collected under different protocols. Therefore, joint analyses of these datasets require
27 robust and consistent inference of ancestry, where a common strategy is to yield an ancestry space
28 generated by a reference dataset. However, such a strategy is sensitive to batch artefacts introduced
29 by different protocols. In this work, we propose a novel robust genome-wide ancestry inference
30 method; referred to as SUGIBS, based on an unnormalized genomic (UG) relationship matrix whose
31 spectral (S) decomposition is generalized by an Identity-by-State (IBS) similarity degree matrix. SUGIBS
32 robustly constructs an ancestry space from a single reference dataset, and provides a robust
33 projection of new samples, from different studies. In experiments and simulations, we show that,
34 SUGIBS is robust against individual outliers and batch artifacts introduced by different genotyping
35 protocols. The performance of SUGIBS is equivalent to the widely used principal component analysis
36 (PCA) on normalized genotype data in revealing the underlying structure of an admixed population
37 and in adjusting for false positive findings in a case-control admixed GWAS. We applied SUGIBS on the
38 1000 Genome project, as a reference, in combination with a large heterogeneous dataset containing
39 auxiliary 3D facial images, to predict population stratified average or ancestry faces. In addition, we
40 projected eight ancient DNA profiles into the 1000 Genome ancestry space and reconstructed their
41 ancestry face. Based on the visually strong and recognizable human facial phenotype, comprehensive
42 facial illustrations of the populations embedded in the 1000 Genome project are provided.
43 Furthermore, ancestry facial imaging has important applications in personalized and precision
44 medicine along with forensic and archeological DNA phenotyping.

45 **Author Summary**

46 Estimates of individual-level genomic ancestry are routinely used in human genetics, epidemiology,
47 and related fields. The analysis of population structure and genomic ancestry can yield significant
48 insights in terms of modern and ancient population dynamics, allowing us to address questions
49 regarding the timing of the admixture events, and the numbers and identities of the parental source
50 populations. Unrecognized or cryptic population structure is also an important confounder to correct
51 for in genome-wide association studies (GWAS). However, to date, it remains challenging to work with
52 heterogeneous datasets from multiple studies collected by different laboratories with diverse
53 genotyping and imputation protocols. This work presents a new approach and an accompanying open-
54 source software toolbox that facilitates a robust integrative analysis for population structure and
55 genomic ancestry estimates for heterogeneous datasets. Given that visually evident and easily
56 recognizable patterns of human facial characteristics covary with genomic ancestry, we can generate
57 predicted ancestry faces on both the population and individual levels as we illustrate for the 26 1000
58 Genome populations and for eight eminent ancient-DNA profiles, respectively.

59 **Introduction**

60 Scientists today have access to large heterogeneous datasets from many studies collected by different
61 laboratories with diverse genotyping and imputation protocols. The joint analysis of these datasets
62 requires a robust and consistent inference of ancestry across all datasets involved, where one
63 common strategy is to yield an ancestry space generated by a reference set of individuals (1). Based
64 on open-research initiatives such as the 1000 Genome project (1KGP) (2), HapMap project (3), Human
65 Genome Diversity project (HGDP) (4), and the POPRES dataset (5), the potential exists to create
66 reference ancestry latent-spaces at different levels of interest, from worldwide inter-continental to
67 fine-scale intra-continental ancestry. A reference ancestry space allows the researcher to collate
68 multiple datasets facilitating analyses that are more advanced. For example, reference ancestry
69 spaces can be used to infer the population structure of samples with family structure or cryptic
70 relatedness (1) and to investigate the genetic similarity between ancient DNA and modern human
71 genomes (6). They also have the potential to correct for population structure in a genome-wide
72 association study (GWAS) on heterogeneous and admixed samples. Of final interest is the association
73 of auxiliary data (e.g. specific phenotypes, such as 3D facial shape used in this work) present in
74 internally collected datasets with ancestral variations captured by a reference space. This requires the
75 projection of the collected datasets into a reference space, followed by an association of the
76 projection scores with the auxiliary data presented.

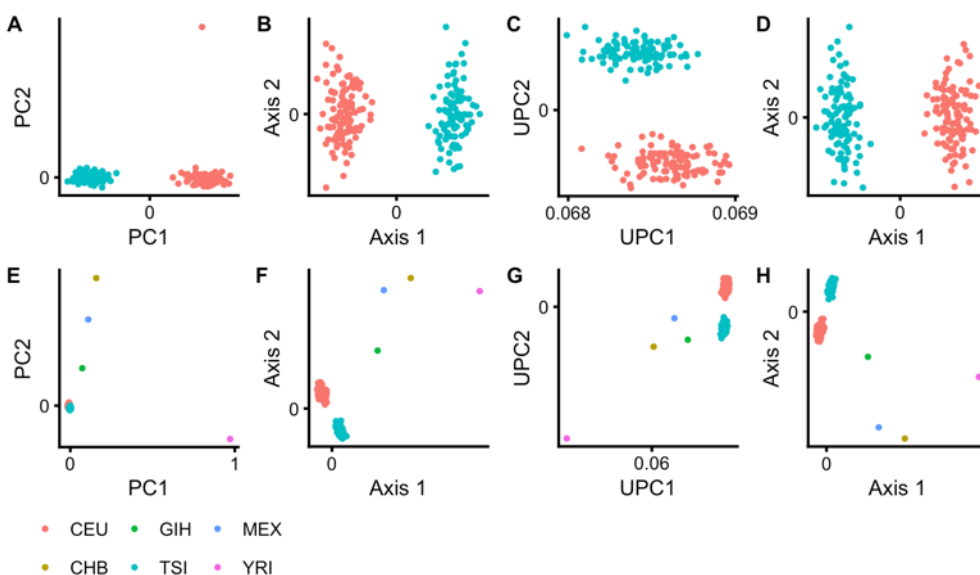
77 Methodologically, the idea is to construct an ancestry latent-space from a reference dataset and to
78 enable the projection of new cases from other datasets that follow the mainstream of the reference
79 dataset. Starting from genome-wide single nucleotide polymorphisms (SNPs), PCA and analogous
80 dimension reduction techniques on normalized genotype data are popular strategies used in this
81 context (7,8). However, in construction of an ancestry space, these approaches are known to be
82 sensitive to outliers (7,9). In addition and more importantly, in projecting new cases onto an ancestry
83 space, PCA produces patterns of misalignment (for example, “shrinkage” patterns where projected
84 cases tend to falsely gravitate towards the center of the ancestry space) due to missing data, missing
85 heterozygotes, and genotyping along with imputation errors, which is misleading without careful
86 interpretation (1). Therefore, stringent quality control and data filters are typically in place to remove
87 individual outliers and SNP data with high missing rates or not in Hardy-Weinberg equilibrium (HWE).
88 However, in heterogeneous datasets, in contrast to homogeneous datasets, such data filters are
89 harder to define, and potentially remove SNP data related to population structure. Furthermore,
90 genotyping and imputation batch artefacts, not detected by quality control and different from one
91 protocol to another, typically remain and still affect an integrative analysis of ancestry.

92 In this work, we propose a novel robust genome-wide ancestry inference (referred to as SUGIBS)
93 based on the spectral (S) decomposition of an unnormalized genomic (UG) relationship matrix
94 generalized by an Identity-by-State (IBS) similarity degree of individuals' matrix. Robustness against
95 outliers, during ancestry space construction, is obtained by absence of specific sample statistics (e.g.
96 allele frequencies). Furthermore, SUGIBS provides a robust projection of new samples, from different
97 studies, onto a reference SUGIBS space. During projection, the IBS similarity degree of individuals to
98 project to individuals in the reference dataset acts as a correcting term for missing genotypes and
99 errors, and most interestingly this correction is on an individual-by-individual basis. We test the
100 robustness of SUGIBS and compare its performance to PCA and Multi-Dimensional Scaling (MDS) in
101 revealing the underlying structure of an admixed population and adjusting for false positive findings

102 in a simulated case-control admixed GWAS. Using the 1KGP as reference dataset, and an additional
 103 heterogeneous dataset containing 3D facial images, we apply SUGIBS to construct ancestry faces that
 104 illustrate the ancestral variation captured in the 1KGP. Additionally, we reconstruct the ancestry faces
 105 for eight high-coverage ancient DNA genomes further illustrating the potential of the work. Based on
 106 the results, our method facilitates a robust integrative analysis for ancestry estimation in
 107 heterogeneous datasets.

108 **Results**

109 In the first experiment, we investigated the robustness of SUGIBS in comparison to traditional
 110 approaches, in particular PCA using normalized or unnormalized genotype data and MDS using IBS
 111 distances as they are implemented in PLINK 1.9 (10), against individual outliers in a reference dataset.
 112 For this purpose, we first selected all unrelated individuals from the CEU and TSI populations in the
 113 HapMap 3 project (Belmont et al., 2003) and used SUGIBS, PCA, unnormalized PCA (UPCA) and MDS
 114 to illustrate the first and second latent dimensions as ancestry components (Figure 1, top row). In
 115 contrast to the traditionally used normalized genotypes in PCA, UPCA used unnormalized genotypes
 116 that were not centralized around the mean and were not standardized to a variance equal to one. As
 117 expected, PCA, MDS and SUGIBS are able to differentiate between both populations along the first
 118 ancestry component. The first component of UPCA seems to aggregate the average pattern of SNPs
 119 instead of the differentiation between two groups. Surprisingly, with PCA a single outlier (NA11917)
 120 that was not expected during the selection of both populations already affected the second ancestry
 121 component. Subsequently, we randomly selected one individual from four different and additional
 122 populations (CHB, GIH, MEX and YRI) as “outliers” in the dataset. Figure 1, bottom row, illustrates the
 123 first two ancestry components of the four methods constructed on the dataset with outliers, where
 124 all four approaches clearly separate the outliers. Using PCA, in contrast to MDS, UPCA and SUGIBS the
 125 clear distinction between CEU and TSI is lost within the first two ancestry components, as they mainly
 126 capture variations due to the outliers. The main reason for robustness in UPCA, MDS and SUGIBS is
 127 that these three methods use unnormalized genotype data and therefore do not rely on specific
 128 sample statistics (e.g. allele frequencies), that otherwise increase the influence of outlier variation.

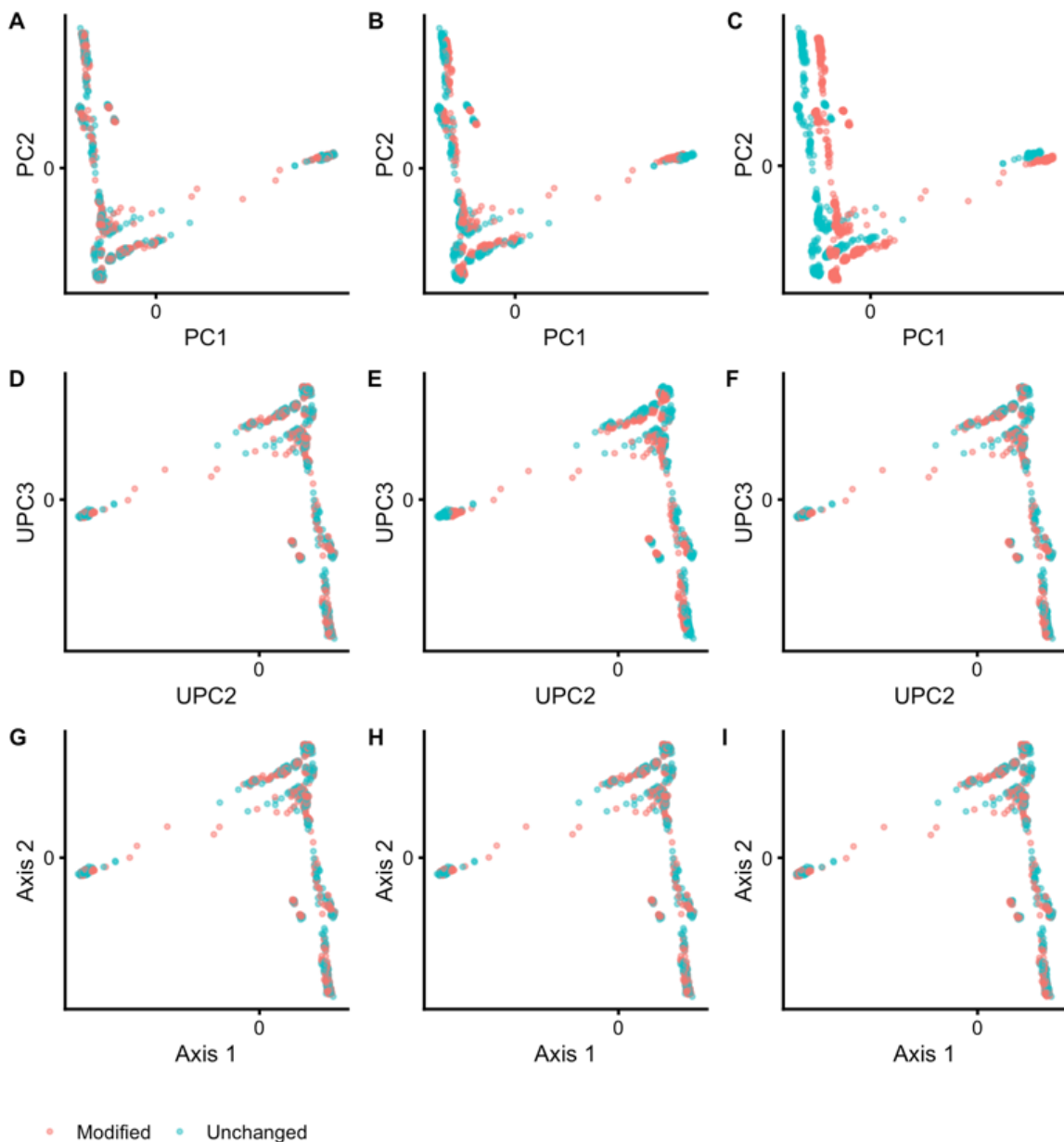


129

130 *Figure 1: Robustness against individual outliers during the construction of an ancestry space. Top row,*
 131 *the first two ancestry components for A) PCA, B) MDS, C) UPCA and D) SUGIBS using the CEU and TSI*

132 *populations from the HapMap 3 project. Bottom row, the first two ancestry components for E) PCA, F)*
133 *MDS, G) UPCA and H) SUGIBS using the CEU and TSI populations from the HapMap 3 project, but with*
134 *randomly selected single individuals from four different and additional populations (CHB, GIH, MEX*
135 *and YRI) as “outliers”.*

136 In a second experiment, we projected (Methods, equation 4) new samples on an ancestry space, based
137 on the 1KGP as reference dataset, to investigate the robustness of SUGIBS in comparison to PCA and
138 UPCA against typical artifacts of different laboratory protocols. Note that, since the first component
139 of UPCA just aggregated the average pattern as seen in experiment 1, we started UPCA from the
140 second component onwards. Also note that, MDS does not allow for a straightforward projection of
141 new samples on a reference space and was therefore excluded. As samples to project, we randomly
142 assigned all 1,043 individuals of 51 populations from the HGDP dataset (4) into two equally-sized
143 samples, one unchanged and one modified, respectively. To investigate the influence of different rates
144 of missing data, we randomly masked 5% of the SNP genotypes as missing in the modified population
145 (See Methods). For the influence of different rates of errors, we partially changed SNP genotypes with
146 minor allele frequency (MAF) less than 5% in the modified population (See Methods). Note that this
147 was done knowing that more imputation errors are observed in SNPs with a MAF of 5% and less (11).
148 We projected both HGDP populations onto the PCA, UPCA and SUGIBS reference spaces as defined by
149 the 1KGP. In PCA, the simulated artefacts generated “shrinkage” and “shifting” patterns of
150 misalignment in the first two projected ancestry components (Figure 2, top row), for missing and
151 erroneous genotypes, respectively. UPCA was only influenced by missing genotypes (Figure 2, middle
152 row). In contrast, SUGIBS was not influenced by missing or erroneous genotypes (Figure 2, bottom
153 row). Figure 3 summarizes the normalized root-mean-square deviations (NRMSD) of the first eight
154 axes of SUGIBS, UPCA and PCA of the modified HGDP population over 100 simulations. SUGIBS is
155 significantly more robust than PCA in the presence of missing and genotyping/imputation errors in
156 new data for which ancestry needs to be inferred, by projecting it into a reference space.

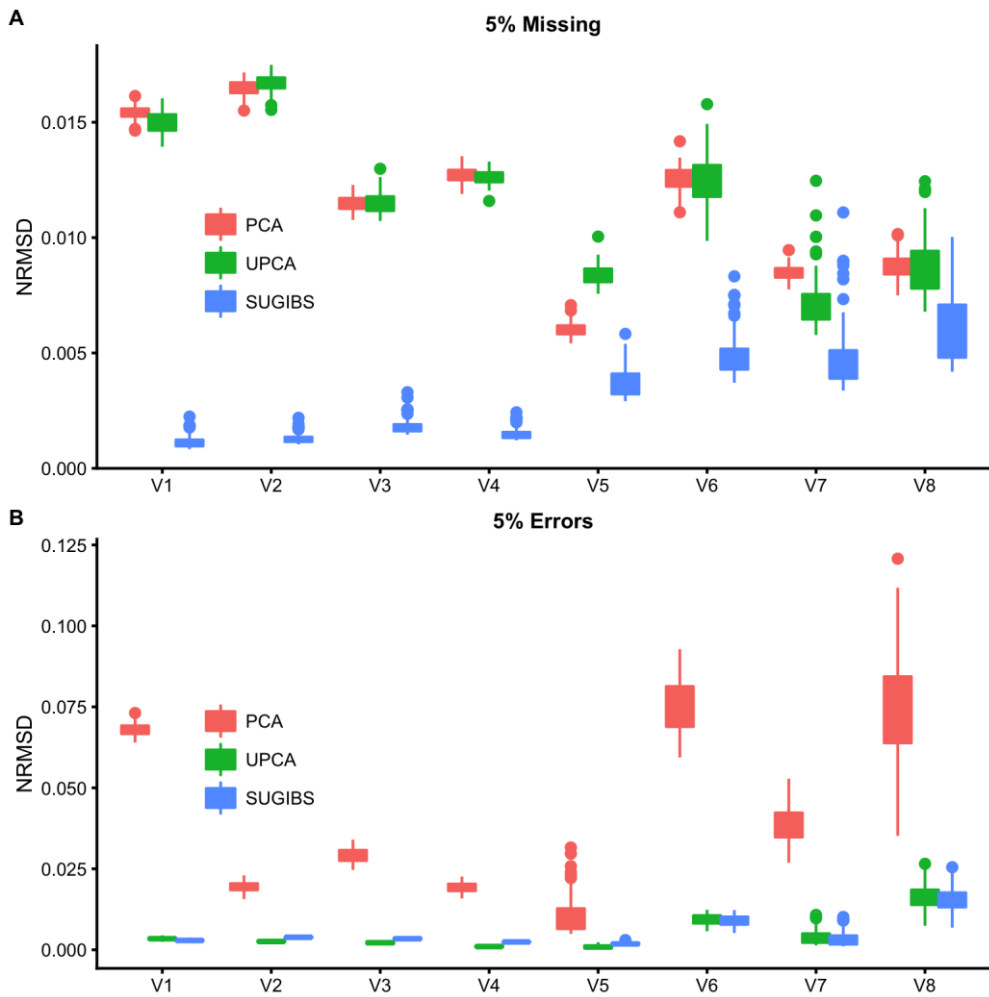


• Modified • Unchanged

157

158 *Figure 2: Robustness against batch artefacts during the projection of samples onto an ancestry space.*
 159 *Top row, the first two ancestry components of PCA using the original genotypes A), missing genotypes*
 160 *B) and modified genotypes C). Middle row, the second and third ancestry components of UPCA using*
 161 *the original genotypes D), missing genotypes E) and modified genotypes F). Bottom row, the first two*
 162 *ancestry components of SUGIBS using the original genotypes G), missing genotypes H) and modified*
 163 *genotypes I).*

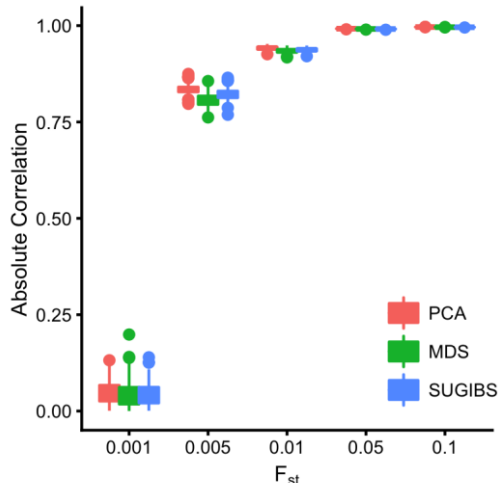
164



167 *Figure 3: Normalized root-mean-square deviation (NRMSD) of the top eight axes of PCA, UPCA and*
 168 *SUGIBS. NRMSD measures the root-mean-square differences (RMSD), for the modified HGDP*
 169 *population only between the scores on ancestry axes generated using the original genotypes (error*
 170 *free) and the modified genotypes (with simulated errors, A) missing genotypes and B) erroneous*
 171 *genotypes). The RMSD values were normalized by the range of the ancestry axes generated using the*
 172 *original genotypes, so that NRMSD of the three methods (PCA, UPCA and SUGIBS) are comparable.*

173 In a third experiment, following the work of Galinsky et al. (12), we investigated the ability of SUGIBS
 174 compared to PCA and MDS in representing admixture. We simulated data at 10,000 random
 175 independent SNPs for 1,000 individuals from a recent admixture of two populations, 50% from each
 176 population on average with divergences $F_{st} = \{0.001, 0.005, 0.01, 0.05, 0.1\}$, from an intra-European
 177 difference to an intercontinental difference (13). Because the admixture contains only one dimension
 178 of population structure, only the first component of variation is of interest. Figure 4 presents the
 179 absolute correlations between the first component of PCA, MDS and SUGIBS and the simulated
 180 ancestry proportions over 100 runs. When the F_{st} divergence between two populations is lower than
 181 0.05, the correlation between the SUGIBS component and the ancestry proportion is similar to that of
 182 MDS, but a little lower than PCA. We noticed that when $F_{st} \leq 0.01$, all three methods have a reduced

183 performance to reveal the underlying admixture and when $F_{st} > 0.01$, all three methods perform
184 perfectly.



185
186 *Figure 4: Capturing simulated admixture in function of F_{st} . X-axis represents the different levels of F_{st}*
187 *investigated. The Y-axis represents the absolute correlation of the first component in PCA, MDS and*
188 *Spectral-IBS with the simulated ancestry proportion. The higher the correlation the better a method is*
189 *able to capture the underlying admixture.*

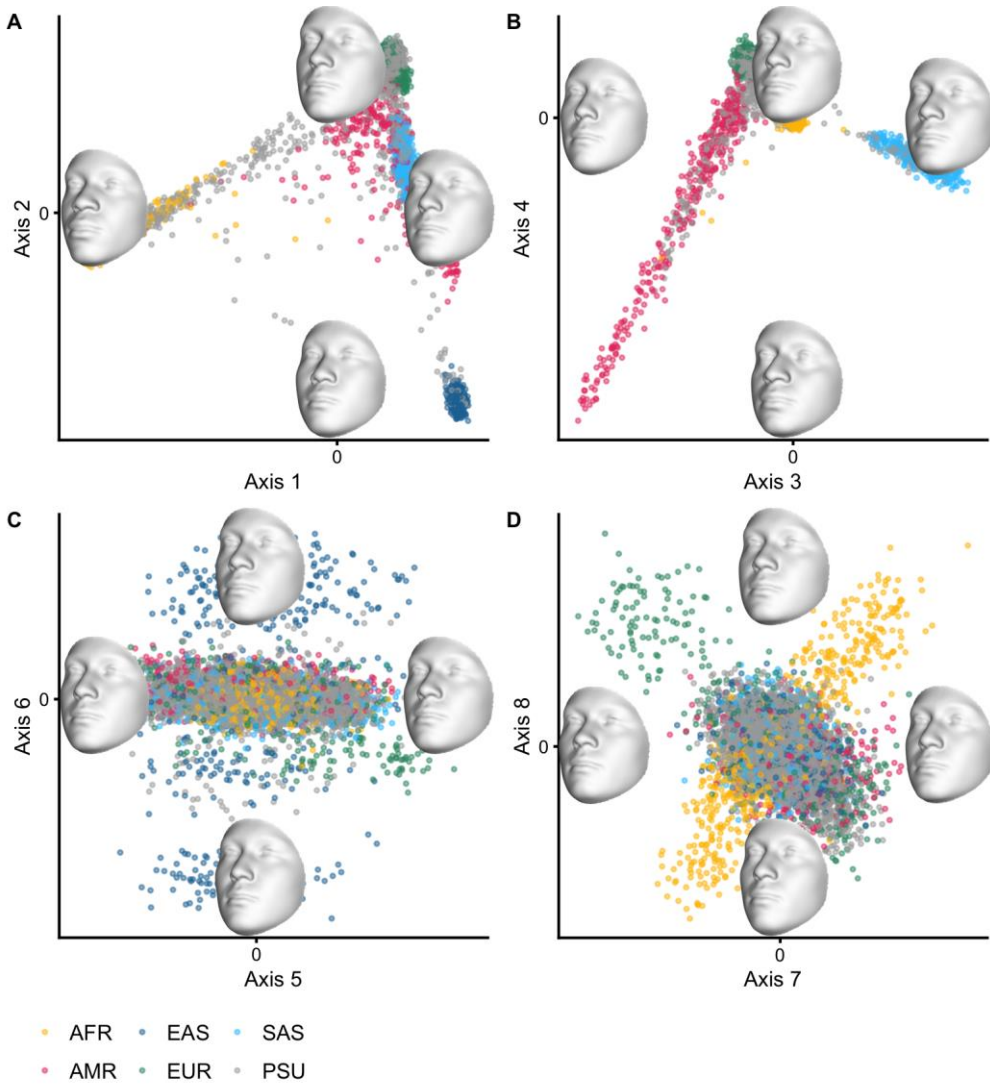
190 Following the work of Price et al. (14), we also simulated a case-control GWAS to investigate if the
191 population structure inferred by SUGIBS can be used for correcting population stratification as a
192 confounder. Only low divergences between the two populations $F_{st} = \{0.001, 0.005, 0.01\}$, were
193 tested, because for larger divergences all three methods would perform the same as deducted from
194 the previous experiment. Tests were conducted with a logistic regression under four different
195 correction scenarios: 1) no population for stratification correction (Naïve), 2) PCA, 3) MDS and 4)
196 SUGIBS, using a likelihood ratio test for the significance of each genetic marker. The experiment was
197 conducted 100 times, with average proportions of SNPs detected as significant shown in Table 1.
198 These results indicate that in a single dimensional population structure, correcting using MDS, SUGIBS
199 and PCA perform similarly, both in terms of Type I error and power. All three methods failed to correct
200 the population stratification when $F_{st} = 0.001$, which is consistent with the failure of the three
201 methods in revealing the admixture structure in the previous experiment. Finally, these results are in
202 line with the results in (14).

203

	Naive	PCA	MDS	SUGIBS
$F_{st} = 0.001$				
Random	0.0002	0.0001	0.0001	0.0001
Differentiated	0.9960	0.4483	0.6370	0.5200
Causal	0.5295	0.4779	0.4865	0.4807
$F_{st} = 0.005$				
Random	0.0009	0.0001	0.0001	0.0001
Differentiated	0.9980	0.0002	0.0003	0.0002
Causal	0.5226	0.4249	0.4255	0.4253
$F_{st} = 0.01$				
Random	0.0030	0.0001	0.0001	0.0001
Differentiated	0.9971	0.0001	0.0001	0.0001
Causal	0.5166	0.4227	0.4230	0.4229

204 *Table 1: Proportion of associations reported as statistically significant ($P < 0.0001$) by logistic
205 regression using a likelihood ratio test. Random SNPs with no association to the disease were
206 generated by simulating random drift with F_{st} divergence. Differentiated SNPs with no association to
207 the disease were generated by assuming population allele frequencies of 0.8 of ancestry 1 and 0.2 of
208 ancestry 2. Causal SNPs were generated by combining a multiplicative disease risk model while
209 simulating the random drift with the same F_{st} as the random SNPs. See methods for more details on
210 the parameters.*

211 Putting SUGIBS to practice, we projected 2,882 unrelated individuals from a large admixed and
212 heterogeneous dataset containing individuals from varying ancestries (the PSU cohort, see Methods)
213 and eight famous ancient DNA samples onto the first 25 SUGIBS axes established from the 26
214 populations in the 1KGP. Shown in Figure 5 and S1 (a), the first two ancestry components separate
215 the African (AFR) and East Asian (ESA) populations from the remaining populations, as indicated by
216 the population labels given in the 1KGP. The next two ancestry components in Figure 5 and S1 (b)
217 separate the South Asian (SAS) population and visualizes the admixture in the Admixed American
218 (AMR) population, respectively. In figure 5 and S1 (c), the sixth ancestry component captures different
219 subpopulations in the EAS population. In Figure 5 and S1 (d), the seventh ancestry component is driven
220 by African subpopulations and the separated European subpopulation on the eighth ancestry
221 component is the population from Finland (FIN). The projected PSU cohort is indicated by gray dots in
222 Figure 5 and S1 and overall it is observed that they overlay well with a wide range of ancestry variations
223 in the 1KGP confirming the heterogeneous and admixed nature of the PSU dataset. However, some
224 populations in the 1KGP are less covered by the PSU cohort, such as the population of Finland in
225 Europe and some African subpopulations on ancestry components seven and eight (Figure 5 d).

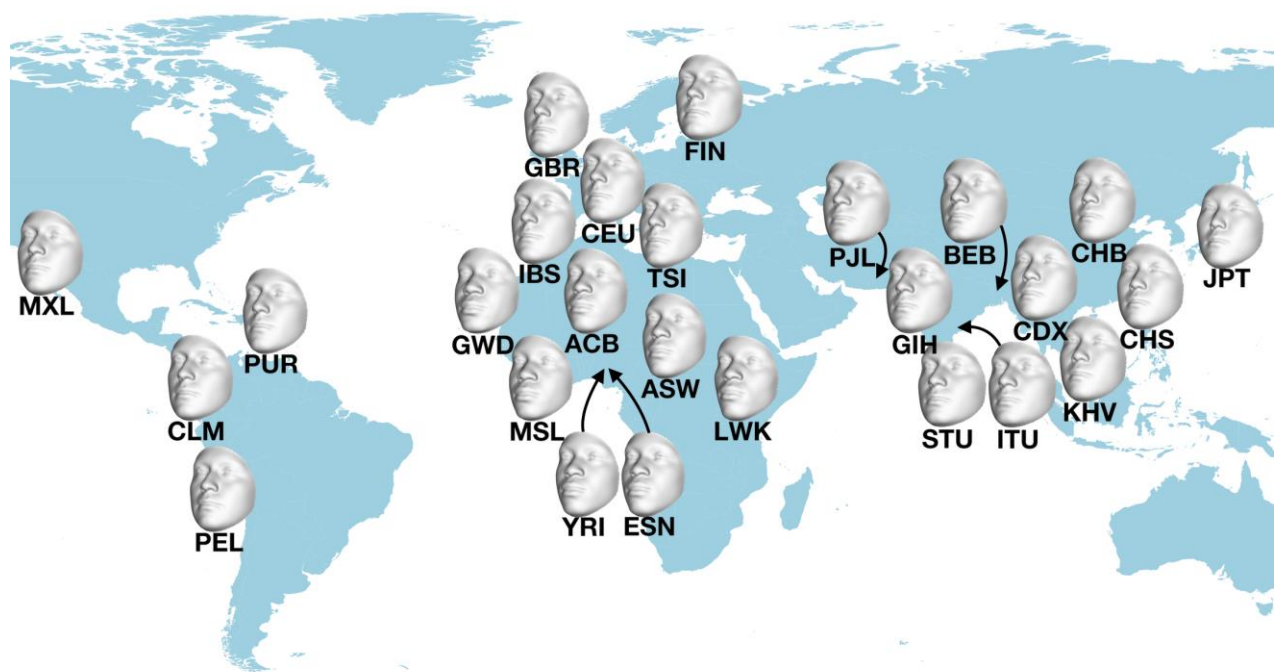


226

227 *Figure 5: Top eight SUGIBS axes of 1KGP and projections of the PSU cohort. Grouped populations of*
 228 *the 1KGP are coloured dots. The projected PSU cohort are represented by grey dots. The faces illustrate*
 229 *opposing variations along each of the ancestry components and are not associated to any of the 1kG*
 230 *populations in particular (these are shown in Figure 6).*

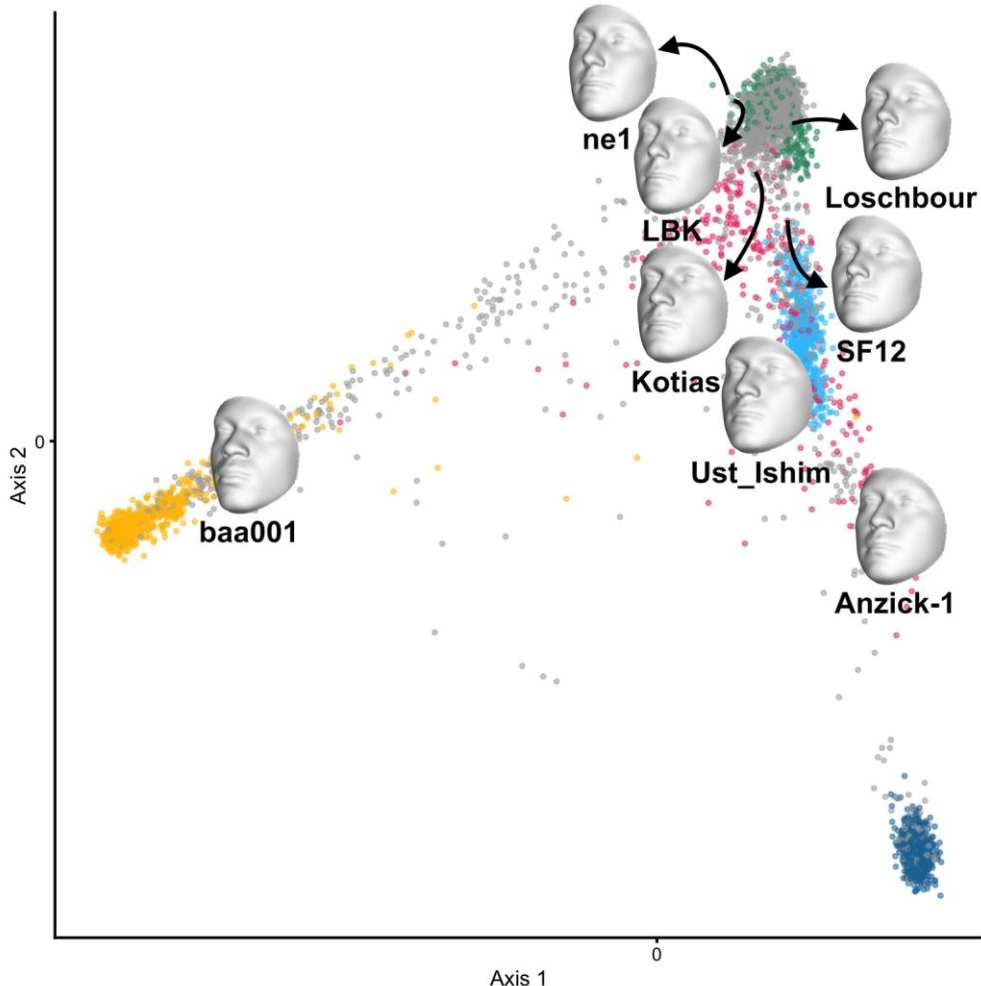
231 Based on the visually strong and recognizable human facial phenotype, we generated comprehensive
 232 illustrations of the population structure embedded in the 1KGP. Using the first 25 SUGIBS scores of
 233 the PSU cohort onto the ancestry components of the 1KGP, we fitted a partial least squares regression
 234 (PLSR) to model facial variations in function of each of the first eight ancestry components (Figure 5).
 235 Strong facial differences are observed for ancestry components 1-4, whilst perceptually smaller
 236 differences occur in components 5-8. This is most likely due to a lower overlap of the PSU cohort with
 237 these ancestry components. Subsequently, we reconstructed the ancestry population average face
 238 from each of the 26 populations in the 1KGP (Figure 6), and ancestry faces specific for eight high-
 239 coverage ancient DNA profiles (Figure 7). The facial images in Figures 5, 6 and 7, are perceptually easy
 240 to confirm the expected variations in facial shape in function of genetic ancestry including admixtures.
 241 For the ancient DNA profiles labeled in Figure 7, it is observed that their projections within the 1kG
 242 ancestry is consistent with the geographical locations where these samples were discovered and what
 243 is currently known about these samples (Supplementary Table S1).

244



245

246 *Figure 6: Ancestry population average faces for each of the 26 populations in the 1KGP positioned*
247 *according to geographical origin. The values for sex, BMI and age in the PLSR model were set to 0*
248 *(sexless), 20 and 25, respectively.*



249

250 *Figure 7: Ancestral facial reconstructions for eight ancient DNA profiles. For these reconstructions, the*
 251 *sex was known from the DNA profile and taken into account in the PLSR model. The values for BMI and*
 252 *age were 20 and 25, respectively.*

253 **Discussion**

254 Accurate inference of population structure and individual global ancestry is of critical importance in
 255 human genetics, epidemiology, and related fields (15,16). The analysis of population structure in itself
 256 can yield significant insights in terms of population dynamics, both in modern and ancient populations
 257 (17–19). Through inspection of ancestry components as well as distances in genetic latent spaces
 258 created by, for example, Principal Component Analysis (PCA), it is possible to infer patterns of gene
 259 flow and population movements through time. Furthermore, the inclusion of various populations in
 260 genome-wide association studies (GWAS) could increase statistical power and make a better
 261 contributions to our understanding of the genetics of complex traits for the human population as a
 262 whole (20). However, the widely used approach of PCA and analogous techniques are sensitive to
 263 outliers, when constructing ancestry spaces, and produce patterns of misalignment due to artifacts of
 264 different laboratory protocols when new samples are projected onto a reference ancestry space
 265 (1,7,9). We propose a robust alternative for genome-wide ancestry inferencing, referred to as SUGIBS.
 266 Our results confirm the erroneous influences in PCA based ancestry estimations that are misleading
 267 without careful interpretation. In constructing an ancestry space SUGIBS, shares the same robustness
 268 against individual outliers as MDS or related spectral graph approaches (21). Furthermore, and more

269 importantly, during dataset projections SUGIBS is robust against typical artefacts from different
270 laboratory protocols. In addition, SUGIBS achieved the same performance, under error-free conditions,
271 as PCA in revealing the underlying structure of an admixed population and avoiding false positive
272 findings in a simulated case-control GWAS with an admixed population.

273 Like MDS and SUGIBS, PCA is also a “spectral” method, in which the edge similarity between
274 individuals is simply the covariance of normalized genotypes, commonly referred to as the genomic
275 relationship matrix (22). However, this covariance similarity used in PCA depends on the allele
276 frequencies as a non-robust sample statistic to normalize the genotypes, which causes sensitivity to
277 individual outliers. Note that in our experiments on PCA without using allele frequencies (UPCA)
278 robustness against individual outliers was observed. Among the “spectral” methods, some other
279 robust alternatives were introduced to infer population structure, including a modified genomic
280 relationship (21,23). MDS or related spectral graph approaches (21) using IBS and Allele Sharing
281 Distance (ASD) similarities between individuals (available in PLINK (10)) are also a robust alternative
282 against individual outliers, as illustrated in our results. IBS and ASD are unnormalized distances, and
283 thus less influenced by outliers. However, MDS and the modified genomic relationship used in (21,23),
284 both lack the ability to project new samples on an already established reference ancestry space.
285 Alternatively, it might be possible to use one of the many robust PCA approaches that have been
286 investigated for general data (24–26) as well as genetic data (27). However, in most study data
287 processing protocols, robust approaches are usually used for outlier detection rather than inferring
288 population structure, which is done by classical PCA after excluding outliers (27). This is for example,
289 a standardly used option in the popular EIGENSOFT software (7). Note that, when establishing an
290 ancestry space from a reference dataset, it remains good practice to identify and remove individual
291 outliers, if they are of no further interest.

292 The main contribution of SUGIBS is robustness against batch artifacts of different laboratory and data
293 processing protocols when projecting new samples onto a reference ancestry space. In the case of
294 missing genotypes, smaller absolute PC scores, and smaller UPC scores are wrongfully generated
295 during the projection of samples. These smaller and decreased scores lead to the “shrinking” and
296 “shifting” patterns as observed in the results. (Note that this is not to be confused with PCA shrinkage
297 due to high dimensional and large-scale data, which is dealt with using shrinkage eigenvalue
298 estimations as recently implemented in EIGENSOFT). However, to correct for this, the projected
299 SUGIBS score matrix is weighted by the reference degree matrix, which captures the similarity
300 between the data to be projected and the reference data (see Methods). This weighting of projected
301 SUGIBS scores equally corrects for the effects of genotyping and imputation errors, as demonstrated
302 in the results. To the best of our knowledge, we are currently not aware of another related approach
303 that offers the same robustness. Based on the results, we argue that SUGIBS is a solid alternative to
304 PCA and MDS and requires less stringent data filters to operate. Our implementation of SUGIBS uses
305 the randomized singular value decomposition algorithm (28), that is also used in FastPCA (12). This
306 makes the algorithm computationally tractable for datasets with tens of thousands of individuals and
307 millions of SNPs. SUGIBS is available as part of an open-source in-house Matlab™ library, referred to
308 as [SNPLIB](#), in which we used PLINK binary file formats as input, and provide FastPCA, logistic GWAS
309 and all other methods and simulations mentioned throughout this work. Furthermore, SUGIBS can
310 easily be incorporated into existing and interesting extensions to derive common ancestry estimations
311 in datasets with non-overlapping genetic variants (1), or genotyping-by-sequencing data (29), or

312 population structure inference in presence of relatedness (30), or in iterative schemes to obtain global
313 to fine-scale ancestry estimations (31).

314 There are a few points of discussion and future investigations. First, a genetic similarity measure
315 between pairs of individuals aims to identify how they are related and different measures exist for
316 ancestry estimations (e.g. IBS, ASD, Identity-by-descent, normalized covariance) (22). Commonly used
317 similarity measures are normalized, just like the traditional approach of PCA on normalized genotype
318 data, to take the genetic composition of individuals along with the rest of the sample into account. A
319 normalization does have the advantage that individuals within the same population are more similar
320 to each other than to individuals in other populations (22). In other words, the distinction between
321 populations increases, which improves population identification by clustering algorithms. However,
322 when the normalization is performed incorrectly clustering efforts might be inaccurate. Furthermore,
323 as seen in our results, such a normalization increases the influence of individual outliers. Finally, in
324 contrast to homogeneous datasets, normalization of genotype data in heterogeneous datasets is
325 challenging depending on whether the dataset is unlabeled or not, imbalanced or not, and with high
326 admixture or not. Starting from unlabeled data, unsupervised clustering approaches such as
327 ADMIXTURE (32) and STRUCTURE (33), iteratively identify the populations individuals belong to and
328 update the normalization accordingly. However, this involves additional parameters to set and tune,
329 the most important one being the amount of clusters expected in the data. Without prior knowledge
330 on how to set these parameters, this can turn into a challenging task. With highly admixture data, any
331 clustering of global ancestry into populations is even questionable. In these situations, only local
332 ancestry estimations, using chromosome painting approaches (34) for example, are meaningful.
333 Alternatively, in the future, we want to investigate the use of a reference ancestry space as
334 constructed in this work, without assigning individuals to specific populations, in estimating
335 normalized genotype data on an individual-by-individual basis. I.e., an ancestry space from
336 unnormalized genotype data is a good first step unbiased by any sample statistics, to further deduct
337 statistics related to individual genotype profiles. For example, (35) propose the Robust Unified Test
338 for Hardy-Weinberg Equilibrium in the context of an admixed population, which also makes use of
339 individual-level adjustments for ancestry. Second, future investigations of the methodology also
340 include the influence of LD pruning and data filtering for SNP selection. Population admixture is one
341 of the main sources for LD between SNPs, therefore we prefer to avoid excessive LD pruning before
342 applying SUGIBS. As stated in (22) any data pruning or filtering is bound to loose information related
343 to population structure. For example, less common variants are typically lost in data filtering, but
344 these might contain valuable information about population structure (22). Since SUGIBS is robust and
345 computationally tractable, any data filtering can be minimized. Third, another future investigation
346 involves the determination of the number of relevant or significant components in SUGIBS, for which
347 we provide a preliminary suggestion that compares the spectrum of the data observed with that of a
348 simulated homogenous dataset assuming linkage equilibrium (LE) and Hardy-Weinberg Equilibrium
349 (Supplementary Text S1).

350 In application of SUGIBS we used the human face, which is a powerful phenotype to visualize and
351 illustrate underlying genetic ancestry variations. Indeed, faces are easy to recognize, interpret, and
352 validate the outcomes based on everyone's expert knowledge in facial perception. The faces
353 illustrating the ancestry components of the 1KGP in this work overlay well with the provided
354 population labels. Therefore, they can also provide a means to interpret ancestry variations in a
355 heterogeneous dataset in absence of population labels. It is important to note that an ancestry face,

356 as referred to in this work, for each of the 26 1kG populations and ancient DNA profiles are faces that
357 reflect a population's or an individual's genetic background and sex. In other words, ancestry faces
358 are not individually specific faces, but average faces that simply visualize the ancestry background of
359 a DNA profile. Related work on facial prediction from DNA (36,37), also show that sex and ancestry
360 are the primary factors driving the estimation of facial shape from DNA.

361 Ancestry facial predictions have good value in a range of applications. In archeology, ancestry faces
362 reconstructed from ancient DNA profiles, as done in this work, is of strong interest. Generally, for
363 ancient DNA profiles, missing data is abundantly present, making SUGIBS an interesting technique to
364 be used. Note that, the ancestry faces are limited to modern facial constructs, due to the
365 contemporary facial data used. However, they can help to bring ancient DNA profiles into the context
366 of present-day populations for which facial images (e.g. open-source facial databases, Google images,
367 etc.) are available but DNA is not. Furthermore, there is a good relationship between the face and the
368 skull (38,39), such that ancestry faces can be used to compare against skeletal remains. In the future,
369 it is of interest to deploy our work on datasets of 3D skeletal craniofacial surfaces extracted from
370 Computer Tomography (CT) or Magnetic Resonance Imaging (MRI). In medicine, and more particularly
371 in oral and maxillofacial surgery, the surgical reconstruction of a patient's face benefits from a proper
372 notion of normal facial shape (40). In the next five to 20 years, whole genome sequencing will become
373 the standard of care in clinics and a patient-specific ancestry face provides a personalized norm of
374 facial shape towards precision medicine in surgical planning. Finally, in forensics, an ancestry facial
375 prediction circumvents the often legally debated reporting of ancestry proportions of a probe DNA
376 profile in a criminal investigation. In France, for example, DNA phenotyping of externally visible traits
377 is legally allowed, since such traits are considered to be public. However, and in contrast, genomic
378 ancestry proportions, as typically reported in forensic DNA testing, is considered to be private
379 information and cannot be used during criminal investigations. We agree that ancestry proportions
380 are not an externally visible characteristic of an individual. The construction of ancestry proportions
381 is also inherently flawed by labelling the individual into so-called parental populations. Furthermore,
382 such numeric information is hard to interpret and use by a forensic investigator. The reconstruction
383 of an ancestry face on the other hand, avoids needing to explicitly label a DNA profile in function of
384 parental populations and provides a visual feedback to an investigator that is perceptually useful, even
385 in admixed cases. A future challenge in forensics does involve the ability to reconstruct ancestry faces
386 using often limited and contaminated DNA material.

387 In conclusion, SUGIBS is a novel approach to construct an ancestry space from a reference dataset and
388 to project new samples from heterogeneous datasets for a consistent and robust inference of
389 individual ancestry. The main contributions involve robustness against outliers during the construction
390 of an ancestry space, and robustness against batch artefacts during the projection of new samples
391 into an ancestry space. Therefore, SUGIBS is a solid alternative to PCA and MDS and facilitates a robust
392 integrative analysis for population structure and ancestry estimations for heterogeneous datasets.
393 Based on the visually strong and recognizable human facial phenotype, comprehensive illustrations of
394 genomic ancestry variations were provided for different populations in the 1KGP and for eight
395 eminent ancient-DNA profiles. Ancestry facial imaging from genome data has interesting future
396 applications in personalized and precision medicine along with forensic and archeological DNA
397 phenotyping.

398

399 **Materials and Methods**

400 **SUGIBS latent-space construction:** Given a dataset with N individuals and M SNPs, we first create an
 401 unnormalized genotype (UG) matrix $\mathbf{X}_{M \times N}$ with additive genotype coding ($aa = -1$, $Aa = 0$, $AA = 1$ and
 402 missing = 0). The UG relationship matrix is then defined as $\mathbf{G} = \frac{1}{M} \mathbf{X}^T \mathbf{X}$. Note that an unnormalized
 403 additive genotype coding has only three values (-1, 0, 1) and does not produce extreme values, which
 404 occurs with normalized additive genotype encoding schemes (typically used in PCA) due to small minor
 405 allele frequencies and in the context of individual outliers.

406 From $\mathbf{W}_{N \times N}$, the IBS similarity matrix of the same dataset used to create \mathbf{G} , the similarity degree of
 407 an individual can be defined as $d_{ii} = \sum_{j=1}^N w_{ij}$. We followed the algorithm implemented in PLINK to
 408 calculate the IBS similarity so that:

IBS	AA	Aa	aa
AA	2	1	0
Aa	1	2	1
aa	0	1	2
N/A	0	0	0

409

410 However, in contrast to the calculations in PLINK, we do not normalize the IBS similarity matrix with
 411 missingness scores. This results in a similarity degree matrix \mathbf{D} defined as the diagonal matrix with
 412 d_{11}, \dots, d_{NN} on the diagonal. We use \mathbf{D} to define generalized eigenvectors $\mathbf{v}_k = (v_{k1}, \dots, v_{kn})^T$ of \mathbf{G}
 413 with corresponding generalized eigenvalues λ_k , and $\lambda_1 \geq \lambda_2 \geq \lambda_3 \geq \dots$:

414
$$\mathbf{Gv}_k = \lambda_k \mathbf{Dv}_k \quad (1)$$

415 Similar to UPCA, the first generalized eigenvector of \mathbf{D} and \mathbf{G} simply represents the average pattern
 416 of all SNPs. Therefore, we start from the second generalized eigenvector and define the k th
 417 component of SUGIBS to be the $k + 1$ th generalized eigenvector of \mathbf{G} and \mathbf{D} , \mathbf{v}_{k+1} .

418 By multiplying $\mathbf{D}^{-\frac{1}{2}}$ on both sides of equation (1), we obtain:

419
$$\mathbf{D}^{-\frac{1}{2}} \mathbf{G} \mathbf{D}^{-\frac{1}{2}} \mathbf{D}^{\frac{1}{2}} \mathbf{v}_k = \lambda_{k+1} \mathbf{D}^{-\frac{1}{2}} \mathbf{v}_k \quad (2)$$

420 Subsequently, we observe that the eigenvector $\mathbf{v}'_k = \mathbf{D}^{\frac{1}{2}} \mathbf{v}_k$ of $\mathbf{D}^{-\frac{1}{2}} \mathbf{G} \mathbf{D}^{-\frac{1}{2}} = \frac{1}{M} \mathbf{D}^{-\frac{1}{2}} \mathbf{X}^T \mathbf{X} \mathbf{D}^{-\frac{1}{2}}$ can be
 421 obtained from the singular value decomposition (SVD) of the matrix $\widehat{\mathbf{X}} = \mathbf{X} \mathbf{D}^{-\frac{1}{2}} = \mathbf{U} \mathbf{\Sigma} \mathbf{V}'^T$, where \mathbf{v}'_k
 422 is also the i th right singular vector with singular value $\sigma_k = \sqrt{M \lambda_{k+1}}$, $\mathbf{\Sigma}$ is a $N \times N$ diagonal matrix, \mathbf{U}
 423 is a $M \times N$ matrix with all the left singular vectors and \mathbf{V}' is a $N \times N$ matrix with all the right singular
 424 vectors.

425 Denoting $\mathbf{U}_k = \{\mathbf{u}_2, \dots, \mathbf{u}_{k+1}\}$ and $\mathbf{\Sigma}_k = \text{diag}\{\sigma_2, \dots, \sigma_{k+1}\}$, the corresponding left singular vectors
 426 and the singular values of the first k SUGIBS components $\mathbf{V}_k = \mathbf{D}^{-\frac{1}{2}} \mathbf{V}'_k = \mathbf{D}^{-\frac{1}{2}} \{\mathbf{v}_2, \dots, \mathbf{v}_{k+1}\}$, we have
 427 the following equation:

428
$$\mathbf{V}_k = \mathbf{D}^{-\frac{1}{2}} \mathbf{V}'_k = \mathbf{D}^{-1} \mathbf{S}_k = \mathbf{D}^{-1} \mathbf{X}^T \mathbf{L}_k = \mathbf{D}^{-1} \mathbf{X}^T \mathbf{U}_k \mathbf{\Sigma}_k^{-1} \quad (3)$$

429 Thus, we denote $\mathbf{L}_k = \mathbf{U}_k \mathbf{\Sigma}_k^{-1}$ as the SUGIBS loading matrix for the first k SUGIBS components and
 430 $\mathbf{S}_k = \mathbf{X}^T \mathbf{U}_k \mathbf{\Sigma}_k^{-1}$ as the unnormalized SUGIBS score matrix.

431 We proposed a preliminary method to select proper number of components which compared the
 432 spectrum of the observed data with that of the simulated data, assuming HWE and Linkage Equilibrium
 433 (see Supplement note).

434 **SUGIBS dataset projection:** Given the SUGIBS loadings \mathbf{L}_k from a reference dataset with N individuals
 435 and M SNPs and given a new dataset with \tilde{N} individuals and the same set of SNPs as the reference
 436 sample, we denote the unnormalized genotype matrix of the new dataset as $\tilde{\mathbf{X}}$. We then define the
 437 reference degree $\tilde{d}_{ii} = \sum_j^N \tilde{w}_{ij}$, where \tilde{w}_{ij} is denoted as the IBS similarity between the i th individual
 438 in the target dataset and the j th individual in the reference dataset. The reference similarity degree
 439 matrix $\tilde{\mathbf{D}}$ of the new dataset is a diagonal matrix with $\tilde{d}_{11}, \dots, \tilde{d}_{\tilde{N}\tilde{N}}$ on the diagonal. For the first k
 440 SUGIBS components, the projected score matrix of the target dataset is then obtained as:

441
$$\tilde{\mathbf{V}}_k = \tilde{\mathbf{D}}^{-1} \tilde{\mathbf{S}}_k = \tilde{\mathbf{D}}^{-1} \tilde{\mathbf{X}}^T \mathbf{L}_k = \tilde{\mathbf{D}}^{-1} \tilde{\mathbf{X}}^T \mathbf{U}_k \mathbf{\Sigma}_k^{-1} \quad (4)$$

442 In equation (4), the reference similarity degree matrix $\tilde{\mathbf{D}}$ acts as a normalization term correcting the
 443 missing genotypes and errors in the samples to be projected. As an example, consider a rare SNP with
 444 major allele A and minor allele G , and an individual with true genotype AA that is wrongfully coded as
 445 GG for that particular SNP. Since the major genotype in the reference data of this SNP is AA , the
 446 number of shared alleles of this SNP between this individual to the majority of individuals in the
 447 reference dataset would reduce from 2 to 0. The unnormalized genotype coding of this person also
 448 changes from 1 to -1. Thus, the influence of such a genotyping error on the unnormalized SUGIBS
 449 score matrix $\tilde{\mathbf{S}}_k$ and the reference similarity degree matrix $\tilde{\mathbf{D}}$ are along the same direction so that the
 450 final SUGIBS scores are corrected by $\tilde{\mathbf{D}}^{-1}$. Other typical batch artefact errors and missing genotypes
 451 in the new dataset are corrected for in a similar way and, most interestingly, this correction is provided
 452 on an individual by individual basis.

453 **Genome-wide common SNP selection across datasets:** We recommend the following procedure to
 454 extract a common set of SNPs between a reference dataset and another dataset being projected, for
 455 constructing SUGIBS ancestry spaces. First, we exclude all the indel, monomorphic, and multi-allelic
 456 SNPs in both the reference dataset and the dataset to project. Subsequently, we extract the list of
 457 SNPs common in both datasets. Based on this list, we further recommend a minor allele frequency
 458 (MAF) filtering with a MAF threshold of 0.01 on the reference dataset using PLINK (10) as a quality
 459 control step. We do not recommend Hardy-Weinberg disequilibrium (HWD) filtering since it is
 460 probably the result of population admixture and thus useful for our purposes (41). Although
 461 population admixture is one of the main sources for LD between SNPs, we still recommend LD pruning
 462 since it is not unusual to have non-uniformly genotyped genomes. Similar to PCA, SUGIBS do not
 463 explicitly model LD between SNPs so that misleading results might be generated without LD pruning.

464 **Individual outlier robustness:** The basic dataset that was used to investigate robustness against
 465 individual outliers in a reference dataset, consists of the individuals from the CEU population (111
 466 individuals) and the TSI population (102 individuals) from the HapMap 3 dataset (3), after excluding
 467 non-founders. We randomly selected one individual as outlier from four other populations (CHB, MEX,

468 GIH, and YRI). These individuals specifically are NA18798 (CHB), NA19740 (MEX), NA21124 (GIH), and
469 NA19262 (YRI). After removing the monomorphic SNPs in each of these three datasets, we built
470 SUGIBS, MDS, UPCA and PCA spaces using 892,338 autosomal SNPs remaining in all three datasets.
471 We intentionally did not perform either minor allele frequency (MAF) filtering or HWE filtering on the
472 SNPs since many rare SNPs and SNPs violating HWE are due to the outliers and were therefore not
473 checked for during the testing for robustness.

474 **Simulated laboratory artefacts:** We used the 1000 Genomes Project dataset (2,504 unrelated
475 individuals from 26 populations) as the reference dataset to infer a PCA, UPCA and SUGIBS based
476 ancestry space. We used the HGDP dataset that analyzed genomic data from 1,043 individuals from
477 around the world as the dataset to project. First, we remapped the HGDP dataset from the NCBI36
478 (hg18) assembly to the GRCh37 (hg19) assembly using the NCBI Genome Remapping Service. Based
479 on the SNP selection procedure for SUGIBS as explained previously, we further performed a LD pruning
480 with a window size of 50, a moving step of 5 and a threshold $r^2 > 0.2$ for several times until no more
481 SNPs were excluded, following (12). LD pruning is a common practice when using PCA. Therefore, we
482 followed this additional step to make the results based on PCA, UPCA and SUGIBS comparable. We
483 finally selected 154,199 autosomal SNPs to construct the PCA, UPCA and SUGIBS ancestry spaces. We
484 then extracted the first eight PCA, UPCA and SUGIBS ancestry components from the reference dataset.
485 After extracting the same set of SNPs in the HGDP dataset, we took care to ensure that the alternate
486 alleles were the same as in the reference dataset.

487 Since PLINK binary file format stores the genotypes of four consecutive individuals in a single byte, we
488 assigned one of every two “bytes” (four individuals) into Population A and the other individuals into
489 Population B of the HGDP dataset. This resulted in 523 individuals for Population A and 520 individuals
490 for Population B. In order to simulate laboratory artefacts, we randomly masked 5% genotype calls as
491 missing and changed 5% genotype calls (e.g., from AA to Aa or aa) of the rare SNPs (MAF < 0.05) in
492 Population A. Random genotype masking and changing were also performed on the “byte” level, i.e.
493 four individuals at a time. For both genotyping masking and changing, we generated 100 datasets to
494 project on the 1kG reference ancestry space. Subsequently, we calculated the root-mean-square
495 deviations (RMSD) between the scores of the top eight PCA, UPCA and SUGIBS axes generated using
496 the original genotypes and the modified genotypes in Population A and further normalized them by
497 the range of the axes generated using the original genotypes so that normalized root-mean-square
498 deviations (NRMSD) across methods are comparable.

499 **Simulated admixed population:** Our admixture simulations were adapted from the section
500 “Simulation Framework” in (12). For a given SNP i , the ancestral allele frequency p_i was sampled from
501 a $Uniform(0.1,0.9)$ distribution. Population allele frequencies were generated by simulating random
502 drift in two populations of fixed effective size N_e for τ generations as p_{i1} and p_{i2} , whose initial values
503 were set to p_i . In each generation, the number of alternate alleles z_{i1} and z_{i2} were sampled from two
504 binomial distributions with $2N_e$ number of trials and p_{i1} and p_{i2} success probabilities. The population
505 allele frequencies were then updated by $p_{i1} = \frac{z_{i1}}{2N_e}$ and $p_{i2} = \frac{z_{i2}}{2N_e}$. For all simulations, population allele
506 frequency simulations were run for 20 generations and the effective population size N_e was calculated
507 for a target F_{st} by $F_{st} = -\log(1 - \frac{\tau}{2N_e})$ (42). This was done for $F_{st} = \{0.001, 0.005, 0.01, 0.05, 0.1\}$,
508 $N_e \approx \{10k, 2k, 1k, 200, 100\}$ with $\tau = 20$.

509 The ancestry proportions α_j were sampled from a $\text{beta}(0.5, 0.5)$ distribution so that the proportion
510 from each ancestry is 50% on average. For a given individual j with ancestry proportion of α_j from
511 Population one and $(1 - \alpha_j)$ from Population two, the individual allele frequency for SNP i was $p_i^j =$
512 $\alpha_j p_{i1} + (1 - \alpha_j) p_{i2}$ and the genotype was sampled from a binomial distribution with 2 trials and p_i^j
513 success probability. The Matlab™ implementations for these simulations are also provided in our
514 SNPLIB library.

515 **Simulated GWAS:** Our GWAS simulation is similar to the one carried out in (14). To simulate a case-
516 control GWAS, we generated 1,000 individuals from a population admixed from two ancestries. The
517 case-control status was simulated using a disease risk proportional to r^α , based on an ancestral risk
518 of $r = 3$. We generated three categories of SNPs (random, differentiating and causal) to compare the
519 performance of PCA, MDS, and SUGIBS in correcting for population stratification. For the first category
520 (random SNPs with no association to the disease), we generated the SNPs by simulating random drift
521 with a certain F_{st} divergence. For the second category (differentiated SNPs with no association), we
522 assumed population allele frequencies of 0.8 for ancestry one and 0.2 for ancestry two. For the third
523 category (causal SNPs), we generated SNPs by combining a multiplicative disease risk model while
524 simulating the random drift with the same F_{st} as the random SNPs.

525 We simulated the case-control status according to (7). For individuals with an ancestry proportion of
526 α from population one and $(1 - \alpha)$ from population two, the case-control status was simulated with
527 the probability of disease equal to $\frac{\log(r)r^\alpha}{2(r-1)}$, which ensures an average value of 0.5 across all the values
528 of α (7).

529 For the case individuals, the population allele frequencies p_{i1} and p_{i2} of the causal SNP i were further
530 updated to $p_{i1}^* = \frac{Rp_{i1}}{1-p_{i1}+Rp_{i1}}$ and $p_{i2}^* = \frac{Rp_{i2}}{1-p_{i2}+Rp_{i2}}$ with a relative risk of $R = 3$, respectively. The
531 Matlab™ implementations for these simulations are also provided in our SNPLIB library.

532 **PSU cohort and 3D facial images:** Study participants in the PSU cohort were recruited in the United
533 States through several studies based at The Pennsylvania State University under Institutional Review
534 Board (IRB) approved protocols (IRB #44929, #45727, #2503, #4320, #32341). 3D facial images were
535 taken using the 3dMD Face (3dMD, Atlanta, GA) and the Vectra H1 (Canfield, Parsippany, NJ) imaging
536 systems. Height and weight were measured using an Accustat stadiometer (Genentech, San Francisco,
537 CA), a clinical scale (Tanita, Arlington Heights, IL), or by self-report. Genotyping was conducted by
538 23andMe (23andMe, Mountain View, CA) on the v4 genome-wide SNP array and on the Illumina Multi-
539 Ethnic Global Array (MEGA). After filtering out SNPs with more than 10% missing genotypes, the
540 intersection of these two arrays compromised of approximately 600K SNPs. We removed individuals
541 with misclassified sex information, missing covariate data, and those with more than 10% missing
542 genotypes. Relatives were identified as pairs of individuals with an identity-by-state (IBS) value of at
543 least 0.8, after which one of each pair was randomly removed, resulting in a set of 2,882 individuals.
544 Genotypes were imputed to the 1000 Genomes Project Phase 3 reference panel, using SHAPEIT2
545 (Delaneau, Marchini, & Zagury, 2012) for prephasing of haplotypes and imputed using the Sanger
546 Imputation Server PBWT pipeline (Durbin, 2014; McCarthy et al., 2016).

547 3D facial images were imported into Matlab™ 2016b in .obj waveform format to perform spatially
548 dense registration (MeshMonk). After importing the images, five positioning landmarks were
549 indicated in the corners of the eye, the tip of the nose and the corners of the mouth to roughly align

550 the images into the same position. Subsequently, the images were cleaned by removing hair, ears,
551 and any dissociated polygons. A symmetrical anthropometric mask (43) of 7,160 landmarks was then
552 mapped onto the pre-processed images (44). This resulted in homologous spatially dense
553 configurations of quasi-landmarks per facial image. Reflected images were created by changing the
554 sign of the x-coordinate of the original mapped images. Both the original and the reflected remapped
555 faces were then superimposed following a generalized Procrustes superimposition to eliminate
556 differences in orientation, position and scale (45). Symmetrized images were created by averaging the
557 original and the reflected images.

558 Image quality control was performed to identify poorly remapped faces using two approaches. First,
559 as described in (46), outlier faces were identified by calculating Z-scores from the Mahalanobis
560 distance between the mean face and each individual face. Faces with Z-scores higher than 2 were
561 manually checked. Second, a score was calculated that reflects the missing data present in the image
562 due to holes, spikes, and other mesh artefacts that can be caused by facial hair or errors during the
563 pre-processing steps, for example. Images with scores indicating a high amount of missing data,
564 indicating large gaps in the mesh, were also manually checked. During the manual check, the images
565 were either classified as images of poor quality or were pre-processed again if possible and mapped
566 again.

567 ***Prediction of ancestry faces:*** Using 69,194 autosomal SNPs overlapping with the PSU cohort and the
568 ancient-DNA profiles, we constructed 25 SUGIBS ancestry components, which is theoretically
569 sufficient to separate 26 populations, from the 1000 Genomes project. Subsequently, we projected
570 the individuals from the PSU cohort and the ancient-DNA profiles onto the 1kG ancestry components.
571 Then, we fitted a partial least-squares regression (PLSR) model using the superimposed 3D facial
572 images with 7,160 quasi-landmarks collected in the PSU cohort as the response variables and the 25
573 projected SUGIBS scores of the PSU cohort together with three covariates (age, sex, and BMI) as the
574 explanatory variables.

575 Given specific ancestry scores on the ancestry components of the 1kG ancestry space, together with
576 age, BMI and sex (-1 (male), 0 (neutral sex) or 1 (female)), the PLSR model was used to predict ancestry
577 faces. To illustrate the ancestry components in Figure 7, we simply varied a single score along each
578 ancestry component separately, while keeping the scores on the other ancestry components fixed and
579 equal to the overall average scores in the PSU cohort together with values for age = 25, BMI = 20, and
580 sex = 0. For each of the 26 populations in the 1KGP, we calculated the average scores on each SUGIBS
581 ancestry component per population. These average scores together with values for age = 25, BMI =
582 20, and sex = 0, were used in the PLSR model to reconstruct the average ancestry faces for each of the
583 26 populations in the 1KGP. Diploid genotypes for the ancient genomes were called using GATK as
584 described in (47). The projected scores of the ancient-DNA profiles were used together with the
585 genome-derived sex values of each of the ancient individuals to reconstruct their ancestry faces in
586 Figure 7.

587 Acknowledgments

588 ***Funding:*** Jiarui Li is in part supported by a Chinese Research PhD scholarship. This investigation was
589 also supported by the KU Leuven, BOF, FWO Flanders (G078518N) and the NIH (1-RO1-DE027023).
590 Kristel Van Steen acknowledges research opportunities offered by F.N.R.S (Convention n° T.0180.13)
591 and by the interuniversity research institute Walloon Excellence in Lifesciences and BIotechnology

592 (WELBIO - Convention de Recherche n° WELBIO-CR-2015S-03R). The collaborators at the Penn State
593 University were supported in part by grants from the Center for Human Evolution and Development
594 at Penn State, the Science Foundation of Ireland Walton Fellowship (04.W4/B643), the United States
595 National Institute Justice (www.nij.gov; 2008-DN-BX-K125), and by the United States Department of
596 Defense (www.defense.gov). Torsten Günther is supported by the Swedish Research Council (2017-
597 05267).

598 **Ethics Statement:** Institutional review board (IRB) approval was obtained at each recruitment site and
599 all participants gave their written informed consent prior to participation; for children, written
600 consent was obtained from a parent or legal guardian. For the PSU cohort, the following local ethics
601 approvals were obtained: State College, PA (IRB #44929 and #4320 New York, NY (IRB #45727);
602 Urbana-Champaign, IL (IRB #13103); Dublin, Ireland; Rome, Italy; Warsaw, Poland; and Porto, Portugal
603 (IRB #32341); and Twinsburg, OH (IRB #2503)

604 **Author contributions:** J.L under supervision of P.C and K.V.S developed the SUGIBS methodology. J.L.
605 together with P.C. designed the experiments with input from K.V.S and M.D.S. J.L. under supervision
606 of P.C. and M.D.S conceptualized and implemented the ancestral facial imaging based on the 1000
607 Genome Project. J.W., T.G., A.Z., R.J.E. and S.W. curated the genomic data, including that of the PSU
608 cohort. M.D.S, J.W., K.I., H.H., N.N., and A.O.C collected and processed the 3D facial image data of the
609 PSU cohort. T.G., E.M.S., and M.J., provided and curated the eight ancient DNA profiles and were
610 involved in the ancestry facial imaging thereof. J.L and P.C wrote the manuscript with extensive input
611 from all co-authors.

612 **Competing interests:** The authors have no financial conflict of interest to report.

613 **Data and materials availability:** Most data used in this work originates from public open-source
614 projects, including the HapMap 3 project, 1000 Genome project and the HGDP dataset. For access to
615 this data, we refer to their respective webpages as indicated under the URL section.

616 The participants comprising the Penn State University dataset (PSU cohort) were not collected with
617 broad data sharing consent. Given the highly identifiable nature of both facial and genomic
618 information and unresolved issues regarding risk to participants, we opted for a more conservative
619 approach to participant recruitment. Broad data sharing of these collections would thus be in legal
620 and ethical violation of the informed consent obtained from the participants. This restriction is not
621 because of any personal or commercial interests. Additional details and a more confined sharing can
622 be requested from M.D.S.

623 An implementation of SUGIBS is freely available (see URL Section). This comprises a Matlab™ toolbox,
624 referred to as SNPLIB, and contains implementations of all the methods and simulations used in this
625 work. We also provide the resulting PLSR model, with demo script, to create Ancestry Facial images
626 for other open or in-house data collections (currently under construction). The spatially-dense facial
627 mapping software, referred to as MeshMonk, is available free of use for academic purposes (see URL
628 Section).

629 **URL's:**

630 HapMap 3 Data: <https://www.genome.gov/10001688/international-hapmap-project/>
631 1000 Genome Project: <http://www.internationalgenome.org/>

632 HGDP dataset: <http://www.cephb.fr/hgdp/>
633 SNPLIB: <https://github.com/jiarui-li/SNPLIB>
634 MeshMonk: <https://github.com/TheWebMonks/meshmonk>
635 NCBI Genome Remapping Service: <https://www.ncbi.nlm.nih.gov/genome/tools/remap>

636

637 References

638

- 639 1. Wang C, Zhan X, Liang L, Abecasis GR, Lin X. Improved Ancestry Estimation for both Genotyping
640 and Sequencing Data using Projection Procrustes Analysis and Genotype Imputation. *Am J Hum
641 Genet.* 2015;
- 642 2. Auton A, Abecasis GR, Altshuler DM, Durbin RM, Bentley DR, Chakravarti A, et al. A global
643 reference for human genetic variation. *Nature.* 2015;526(7571):68–74.
- 644 3. Belmont JW, Hardenbol P, Willis TD, Yu F, Yang H, Ch'Ang LY, et al. The international HapMap
645 project. *Nature.* 2003 Dec;426(6968):789–96.
- 646 4. Li JZ, Absher DM, Tang H, Southwick AM, Casto AM, Ramachandran S, et al. Worldwide human
647 relationships inferred from genome-wide patterns of variation. *Science.* 2008;319(5866):1100–
648 4.
- 649 5. Nelson MR, Bryc K, King KS, Indap A, Boyko AR, Novembre J, et al. The Population Reference
650 Sample, POPRES: A Resource for Population, Disease, and Pharmacological Genetics Research.
651 *Am J Hum Genet.* 2008;
- 652 6. Skoglund P, Malmström H, Omrak A, Raghavan M, Valdiosera C, Günther T, et al. Genomic
653 diversity and admixture differs for stone-age Scandinavian foragers and farmers. *Science.*
654 2014;
- 655 7. Price AL, Patterson NJ, Plenge RM, Weinblatt ME, Shadick NA, Reich D. Principal components
656 analysis corrects for stratification in genome-wide association studies. *Nat Genet.*
657 2006;38(8):904–9.
- 658 8. Patterson N, Price AL, Reich D. Population structure and eigenanalysis. *PLoS Genet.*
659 2006;2(12):2074–93.
- 660 9. Clayton DG, Walker NM, Smyth DJ, Pask R, Cooper JD, Maier LM, et al. Population structure,
661 differential bias and genomic control in a large-scale, case-control association study. *Nat
662 Genet.* 2005 Nov;37(11):1243–6.
- 663 10. Purcell S, Neale B, Todd-Brown K, Thomas L, Ferreira MAR, Bender D, et al. PLINK: A Tool Set
664 for Whole-Genome Association and Population-Based Linkage Analyses. *Am J Hum Genet.*
665 2007;81(3):559–75.
- 666 11. Mitt M, Kals M, Pärn K, Gabriel SB, Lander ES, Palotie A, et al. Improved imputation accuracy of
667 rare and low-frequency variants using population-specific high-coverage WGS-based
668 imputation reference panel. *Eur J Hum Genet.* 2017 Jun 12;25(7):869–76.
- 669 12. Galinsky KJ, Bhatia G, Loh PR, Georgiev S, Mukherjee S, Patterson NJ, et al. Fast Principal-
670 Component Analysis Reveals Convergent Evolution of ADH1B in Europe and East Asia. *Am J
671 Hum Genet.* 2016;98(3):456–72.

672 13. Nelis M, Esko T, Mägi R, Zimprich F, Toncheva D, Karachanak S, et al. Genetic structure of
673 europeans: A view from the north-east. *PLoS ONE*. 2009;

674 14. Price AL, Zaitlen NA, Reich D, Patterson N. New approaches to population stratification in
675 genome-wide association studies. *Vol. 11, Nature Reviews Genetics*. 2010. p. 459–63.

676 15. Bauchet M, McEvoy B, Pearson LN, Quillen EE, Sarkisian T, Hovhannesyan K, et al. Measuring
677 European Population Stratification with Microarray Genotype Data. *Am J Hum Genet*.
678 2007;80(5):948–56.

679 16. Cavalli-Sforza LL. Population Structure and Human Evolution. *Proc R Soc B Biol Sci*.
680 1966;164(995):362–79.

681 17. Cavalli-Sforza LL, Monozzi P, Piazza A. *The History and Geography of Human Genes*. Abridged e.
682 Princeton University Press. Princeton, NJ: Princeton University Press; 1994.

683 18. Rosenberg NA, Pritchard JK, Weber JL, Cann HM, Kidd KK, Zhivotovsky LA, et al. Genetic
684 structure of human populations. *Science*. 2002;298(5602):2381–5.

685 19. Nielsen R, Akey JM, Jakobsson M, Pritchard JK, Tishkoff S, Willerslev E. Tracing the peopling of
686 the world through genomics. *Nature*. 2017;541(7637):302–10.

687 20. Rosenberg NA, Huang L, Jewett EM, Szpiech ZA, Jankovic I, Boehnke M. Genome-wide
688 association studies in diverse populations. *Nat Rev Genet*. 2010;11(5):356–66.

689 21. Lee AB, Luca D, Roeder K. A spectral graph approach to discovering genetic ancestry. *Ann Appl
690 Stat*. 2012;6(1):179–202.

691 22. Lawson DJ, Falush D. Population Identification Using Genetic Data. *Annu Rev Genomics Hum
692 Genet*. 2012;13(1):337–61.

693 23. Zhang J, Niyogi P, Mcpeak MS. Laplacian eigenfunctions learn population structure. *PLoS ONE*.
694 2009;4(12).

695 24. Croux C, Filzmoser P, Oliveira MR. Algorithms for Projection-Pursuit robust principal
696 component analysis. *Chemom Intell Lab Syst*. 2007 Jun;87(2):218–25.

697 25. Croux C, Ruiz-Gazen A. High breakdown estimators for principal components: the projection-
698 pursuit approach revisited. *J Multivar Anal*. 2005 Jul;95(1):206–26.

699 26. Maronna R. Principal components and orthogonal regression based on robust scales.
700 *Technometrics*. 2005;

701 27. Liu L, Zhang D, Liu H, Arendt C. Robust methods for population stratification in genome wide
702 association studies. *BMC Bioinformatics*. 2013 Apr 19;14:132.

703 28. Halko N, Martinsson P-G, Tropp JA. Finding structure with randomness: Probabilistic algorithms
704 for constructing approximate matrix decompositions. *SIAM Rev*. 2009;53(2):217–88.

705 29. Dodds KG, McEwan JC, Brauning R, Anderson RM, Stijn TC, Kristjánsson T, et al. Construction of
706 relatedness matrices using genotyping-by-sequencing data. *BMC Genomics*. 2015;

707 30. Conomos MP, Miller MB, Thornton TA. Robust inference of population structure for ancestry
708 prediction and correction of stratification in the presence of relatedness. *Genet Epidemiol*.
709 2015;

710 31. Chaichoompu K, Yazew FA, Tongsima S, Shaw PJ, Sakuntabhai A, Van Steen K. IPCAPS: an R
711 package for iterative pruning to capture population structure. 2017.

712 32. Alexander DH, Novembre J, Lange K. Fast model-based estimation of ancestry in unrelated
713 individuals. *Genome Res*. 2009;19(9):1655–64.

714 33. Pritchard JK, Stephens M, Rosenberg NA, Donnelly P. Association Mapping in Structured
715 Populations. *Am J Hum Genet*. 2000;67(1):170–81.

716 34. Lawson DJ, Hellenthal G, Myers S, Falush D. Inference of population structure using dense
717 haplotype data. *PLoS Genet*. 2012;8(1).

718 35. Kwong A, Kang HM, Program TT-O for PM. A robust unified test for Hardy-Weinberg
719 equilibrium in arbitrarily structured populations. In: ASHG 2018 Annual Meeting. ASHG 2018
720 Annual Meeting; 2018.

721 36. Claes P, Hill H, Shriver MD. Toward DNA-based facial composites: Preliminary results and
722 validation. *Forensic Sci Int Genet*. 2014;

723 37. Lippert C, Sabatini R, Maher MC, Kang EY, Lee S, Arikian O, et al. Identification of individuals by
724 trait prediction using whole-genome sequencing data. *Proc Natl Acad Sci*. 2017;

725 38. Claes P, Vandermeulen D, De Greef S, Willems G, Clement JG, Suetens P. Computerized
726 craniofacial reconstruction: Conceptual framework and review. *Forensic Science International*.
727 2010.

728 39. Claes P, Vandermeulen D, De Greef S, Willems G, Clement JG, Suetens P. Bayesian estimation
729 of optimal craniofacial reconstructions. *Forensic Sci Int*. 2010;

730 40. Claes P, Walters M, Gillett D, Vandermeulen D, Clement JG, Suetens P. The normal-equivalent:
731 A patient-specific assessment of facial harmony. *Int J Oral Maxillofac Surg*. 2013;

732 41. Deng HW, Chen WM, Recker RR. Population admixture: Detection by Hardy-Weinberg test and
733 its quantitative effects on linkage-disequilibrium methods for localizing genes underlying
734 complex traits. *Genetics*. 2001;

735 42. Bhatia G, Patterson N, Pasaniuc B, Zaitlen N, Genovese G, Pollack S, et al. Genome-wide
736 comparison of African-ancestry populations from CARE and other cohorts reveals signals of
737 natural selection. *Am J Hum Genet*. 2011;89(3):368–81.

738 43. Claes P, Walters M, Clement J. Improved facial outcome assessment using a 3D anthropometric
739 mask. *Int J Oral Maxillofac Surg*. 2012;

740 44. Snyders J, Claes P, Vandermeulen D, Suetens P. Non-rigid surface registration algorithms:
741 Technical details and comparison. 2014.

742 45. Rohlf FJ, Slice D. Extensions of the Procrustes Method for the Optimal Superimposition of
743 Landmarks. *Syst Zool*. 1990;

744 46. Claes P, Roosenboom J, White JD, Swigut T, Sero D, Li J, et al. Genome-wide mapping of global-
745 to-local genetic effects on human facial shape. *Nat Genet*. 2018;

746 47. Günther T, Malmström H, Svensson EM, Omrak A, Sánchez-Quinto F, Kilinç GM, et al.
747 Population genetics of Mesolithic Scandinavia: Investigating early postglacial migration routes
748 and high-latitude adaptation. *PLOS Biol*. 2018 Jan 9;16(1):e2003703.

749

750

751 **Supplementary Materials:**

752

753 **Supplementary Table S1:** Information and references for each of the 8 ancient DNA profiles.

754

755 **Supplementary Figure S1:** Top eight SUGIBS axes of 1KGP and projections of the PSU cohort

756

757 **Supplementary Text S1:** Determination of the number of relevant or significant components

758

759

760 **Figure Captions:**

761
762 **Figure 1:** Robustness against individual outliers during the construction of an ancestry space. Top
763 row, the first two ancestry components for A) PCA, B) MDS, C) UPCA and D) SUGIBS using the
764 CEU and TSI populations from the HapMap 3 project. Bottom row, the first two ancestry
765 components for E) PCA, F) MDS, G) UPCA and H) SUGIBS using the CEU and TSI populations
766 from the HapMap 3 project, but with randomly selected single individuals from four different
767 and additional populations (CHB, GIH, MEX and YRI) as “outliers”.

768
769 **Figure 2:** Robustness against batch artefacts during the projection of samples onto an ancestry
770 space. Top row, the first two ancestry components of PCA using the original genotypes A),
771 missing genotypes B) and modified genotypes C). Middle row, the second and third ancestry
772 components of UPCA using the original genotypes D), missing genotypes E) and modified
773 genotypes F). Bottom row, the first two ancestry components of SUGIBS using the original
774 genotypes G), missing genotypes H) and modified genotypes I).

775
776 **Figure 3:** Normalized root-mean-square deviation (NRMSD) of the top eight axes of PCA, UPCA and
777 SUGIBS. NRMSD measures the root-mean-square differences (RMSD), for the modified HGDP
778 population only between the scores on ancestry axes generated using the original genotypes
779 (error free) and the modified genotypes (with simulated errors, A) missing genotypes and B)
780 erroneous genotypes). The RMSD values were normalized by the range of the ancestry axes
781 generated using the original genotypes, so that NRMSD of the three methods (PCA, UPCA and
782 SUGIBS) are comparable.

783
784 **Figure 4:** Capturing simulated admixture in function of F_{st} . X-axis represents the different levels of F_{st}
785 investigated. The Y-axis represents the absolute correlation of the first component in PCA, MDS
786 and Spectral-IBS with the simulated ancestry proportion. The higher the correlation the better
787 a method is able to capture the underlying admixture.

788
789 **Figure 5:** Top eight SUGIBS axes of 1KGP and projections of the PSU cohort. Grouped populations of
790 the 1KGP are coloured dots. The projected PSU cohort are represented by grey dots. The faces
791 illustrate opposing variations along each of the ancestry components and are not associated to
792 any of the 1kG populations in particular (these are shown in Figure 6).

793
794 **Figure 6:** Ancestry population average faces for each of the 26 populations in the 1KGP positioned
795 according to geographical origin. The values for sex, BMI and age in the PLSR model were set to
796 0 (sexless), 20 and 25, respectively.

797
798 **Figure 7:** Ancestral facial reconstructions for eight ancient DNA profiles. For these reconstructions,
799 the sex was known from the DNA profile and taken into account in the PLSR model. The values
800 for BMI and age were 20 and 25, respectively.